Kinetic theory of ultrasubsonic fermion systems and applications to flat-band magic-angle twisted bilayer graphene transport

Seth M. Davis [*] and Sankar Das Sarma

Condensed Matter Theory Center and Joint Quantum Institute, Department of Physics, University of Maryland, College Park, Maryland 20742, USA

The only kinematically allowed phonon-scattering events for bands of subsonic fermions ($v_F < v_p$) are interband transitions, leading to different low-T transport physics in nearly flat-band systems (NFBs) than in the typical supersonic case. We apply a kinetic theory of phonon-limited transport to a generic two-band system of subsonic fermions, deriving formulas for relaxation times and resistivity that are accurate in the "ultrasubsonic" limit defined by small v_F/v_p and small band separation. We predict regimes of $\rho \propto T$, $\rho \propto T^2$, and perfect conductivity. Our theory predicts linear-in-T resistivity down to a crossover temperature that is suppressed from its supersonic analog by a factor of v_F/v_p, offering a different explanation for low-T "strange metal" behavior observed in NFBs. Understanding NFBs thus requires updated expectations for "normal" transport physics.

Rapid progress in the fabrication and manipulation of layered two-dimensional van der Waals heterostructures has led to an unprecedented ability to engineer nearly flat-band (NFB) electronic systems, which have already displayed a wealth of exotic phenomena [1–41]. However, all solid-state systems contain phonons. To understand observations of novel physics in solid-state NFB systems, it is important to understand how phonons interact with NFB fermions. This work focuses on one aspect: When the fermions in question are *subsonic* ($v_F < v_p$), kinematics requires that all single-phonon scattering processes are interband transitions, with consequences on the low-T transport physics.

The prime example of the NFB systems is magic-angle twisted bilayer graphene (MATBLG). MATBLG has been found to exhibit superconductivity (SC) proximate to strongly correlated insulating states [7–13,22] and has been reported to exhibit a linear-in-T "strange-metal"-like resistivity over a large range of dopings and temperatures [9,26–28], sometimes down to temperatures as low as 50 mK [42]. These phenomena have inspired analogy between MATBLG and the cuprate high-T_c SCs, as well as speculation that SC in MATBLG might be driven by strong correlation physics. However, phonon-based theories of SC [43,44] and high-T transport [28,43,45] in MATBLG have been put forth that give generally good quantitative agreement with experiment. It is thus imperative to understand whether low-T, linear-in-T transport in MATBLG is indeed arising from a strange metal state.

The standard kinetic theory of acoustic phonon scattering is exceptionally accurate in describing transport in layered graphene systems (as well as in normal metals and semiconductors) at temperatures above a few Kelvin [43,45–47], and accurately describes TBLG transport away from the magic angle [43,45]. In this work, we apply the same framework to NFB systems at asymptotically low T, extending the kinetic theory well beyond its regime of proven validity. Remarkably, the familiar theory predicts qualitatively different low-T transport physics for subsonic fermions than it does for the (standard) supersonic alternative, due entirely to the kinematic differences between the two limits.

We develop a transport theory for a generic two-band fermion system in the "ultrasubsonic" (USS) limit, which we define as the double limit of small v_F/v_p and small band separation. This limit allows an analytical solution to the Boltzmann transport equation. We show that the interband nature of subsonic fermion scattering manifests an exponentially divergent relaxation time at low temperatures, in contrast with the familiar $\tau \propto T^{-4}$ Bloch-Grüneisen (BG) power law applicable to supersonic fermions. The divergence in relaxation time is capable of perfectly balancing the thermodynamic suppression of states away from the Fermi level, leading to a nonintuitive physical picture in which states far from the Fermi level contribute meaningfully to transport. This scenario produces a linear-in-T resistivity over a wide range of T, and down to a temperature much lower than the BG paradigm of supersonic fermion bands would suggest possible. The divergence in relaxation time can also drive the system to perfect conductivity at asymptotically low T, mimicking a SC transition. We also note that the geometry of isolated NFBs can manifest a mid-T, $\rho \propto T^2$ power law. All these features are consistent with the hitherto unexplained phenomenology of MATBLG transport.

There are reasons to suspect that the kinetic theory of acoustic-phonon-limited transport may not apply well to NFB systems. Nevertheless, it is important to understand the predictions of naive kinetic theory for NBF systems. The fact that our theory gives a simple and concrete mechanism for robust linear-in-T resistivity is noteworthy, given that this is the primary signature of the "strange-metal" state. Further, it is interesting that phonon scattering in subsonic fermion

---

[*]sethdavis108@gmail.com

bands can also generate regimes of $\rho \propto T^2$ resistivity, often assumed to arise from electron-electron scattering in Fermi liquids, and regimes of perfect conductivity that mimic the behavior of superconductivity. While an accurate, quantitative treatment of realistic NFB electron-phonon physics is beyond reach, the atypical kinematics of subsonic fermions could be a key ingredient to understanding transport in NFB systems, which our approach is able to fully capture. Although our theory has MATBLG in mind, we work with a general USS model and our results apply widely to NFB systems.

I. PHONON SCATTERING OF SUPERSONIC AND SUBSONIC FERMIONS

In an electron-phonon scattering process, conservation of energy and momentum defines a "scattering manifold" of Bloch states that a given initial state can scatter to. The maximum energy difference between a Bloch state on the scattering manifold and the initial state defines the Bloch-Grüneisen temperature T_{BG} [48] [Fig. 1(a)]. When $T \gg T_{BG}$, enough phonon modes will be populated that all kinematically allowed scattering events are possible. This is the so-called "equipartition regime," which is characterized by a linear-in-T scattering rate for each Bloch state, usually giving a linear-in-T resistivity above T_{BG}. On the other hand, when $T \ll T_{BG}$, only low-energy phonon modes are available and scattering is restricted to a small neighborhood of the initial state. This is what gives rise to the famous low-T $\tau \propto T^{-(d+2)}$ power law in the Bloch-Grüneisen regime (where d is the spatial dimension). Crucially, when $v_F > v_p$, the scattering manifold is smoothly connected to the original state, allowing arbitrarily small-momentum scattering events. As a result, the BG regime holds all the way to zero temperature. In single-layer graphene and in normal metals, $v_F/v_p \approx O(10^2)$ or larger.

However, when the Bloch state in question is subsonic, all phonon scattering processes are interband processes and the scattering manifold determined by energy-momentum conservation is necessarily disconnected from the original state [see Fig. 1(c)]. This is the crucial difference between the supersonic and subsonic cases. This implies minimum allowed energy transfer (ΔE_{min}) in scattering events, which defines another temperature scale applicable for subsonic scattering $T_{SS} \approx \Delta E_{min}/k_B$. Since the phonons obey Bose statistics, the availability of the phonons with energies above ΔE_{min} is exponentially suppressed for T below T_{SS}, and we expect a crossover to a regime in which the entire scattering manifold is inaccessible. Below T_{SS}, the exponential suppression of the phonons needed for scattering causes the relaxation time of the Bloch state to diverge *exponentially* as $T \to 0$ (instead of $\tau \propto T^{-4}$ as in the supersonic BG regime).

II. BASIC KINETIC THEORY

The well-known fundamental equation giving the resistivity in terms of the *relaxation times* τ_S is [43,45–47,49–51]

$$\frac{\delta^{ij}}{\rho} = \frac{e^2}{k_B T} \frac{1}{\mathcal{A}} \sum_S \tau_S v_S^i v_S^j f(\varepsilon_S)[1 - f(\varepsilon_S)], \quad (1)$$
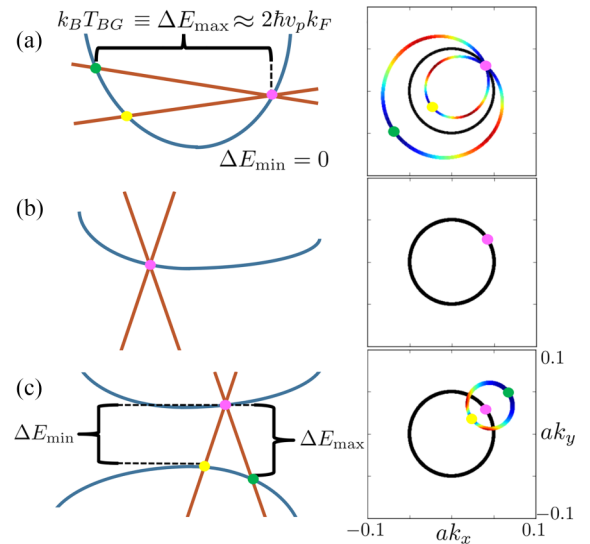
FIG. 1. Key aspects of phonon scattering for subsonic fermions can be understood from simple schematic figures. Above we depict three simple cases: (a) The usual case of scattering of a supersonic fermion in a single-band system, (b) the scattering of a subsonic fermion in a single-band system, and (c) the scattering of a subsonic fermion in a double-band system. In each case, the left side of the figure shows a cross section of a fermion band structure (blue), with momentum on the horizontal axis and energy on the vertical axis. We pick an "initial" Bloch state (pink) and superimpose on it the Debye dispersion of the acoustic phonons (orange). Due to energy and momentum conservation, a fermion in the initial state (pink) can only scatter to one of the intersection points of the fermion and phonon bands (e.g., green or yellow). The intersection of the fermion band with the Debye cone defines the *scattering manifold*. On the right side of the figure, we give a momentum space plot of the scattering manifold geometry. The pink dot again is the initial state, the black curve represents the Fermi surface, and the colored curves mark the scattering manifolds. The green and yellow points mark corresponding locations on the scattering manifolds. In (a), we see that the maximum allowed energy transfer defines T_{BG}, and that the scattering manifold connects smoothly to the initial state, so that arbitrarily small energy transfers are allowed. In (b), we see that a single-band system of subsonic fermions does not allow single-phonon scattering events. This follows from the simple fact that the fermion and phonon dispersions only intersect at the initial state, and thus there is no scattering manifold. In (c) see that in multiband subsonic fermion system, the phonon scattering is necessarily interband, and the scattering manifold is not connected to the initial state. In addition to a maximum allowed energy difference defining a Bloch-Grüneisen scale, there is also a minimum allowed energy difference.

where $\mathcal{A}$ is the area of the system, $f(\varepsilon)$ is the Fermi-Dirac distribution, the sum runs over the (moiré) Bloch states S, and v_S, ε_S, and τ_S are the Fermi velocity, energy, and relaxation time of the state S, respectively. The relaxation times are determined from a self-consistent integral equation, derived from the Boltzmann equation, which depends on the details of the phonon couplings. Since we do not use this directly in the main text, we present these details in the Appendixes.
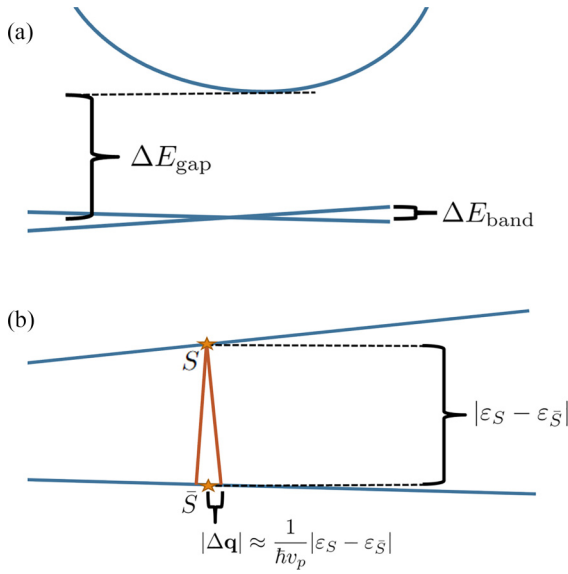
FIG. 2. In (a) we depict the scenario of an NFB system isolated from the rest of the band structure by a sizable energy gap. Phonon scattering can produce a $\rho \propto T^2$ resistivity power law for $\Delta E_{\text{band}} \ll k_B T \ll \Delta E_{\text{gap}}$ in this band geometry. In (b), we depict the band geometry of the ultrasubsonic limit, defined by $v_F \ll v_p$ and small band separation.

III. EQUIPARTITION REGIME: $\rho \propto T^2$

When $T \gg T_{\text{BG}}$ ("equipartition regime"), the inverse relaxation times scale linearly with temperature:

$$\tau_S = \frac{c_S}{k_B T} + O\left(\frac{\Delta\varepsilon}{(k_B T)^3}\right), \qquad (2)$$

where c_s are some (T, μ)-independent proportionality constants that depend on the details of the band structure. In the usual case, the high-T, linear-in-T power law follows directly from this linear scattering rate. However, in the case of NFBs separated from all other bands by a large energy gap, there is a mid-T regime in which T is larger than the NFB bandwidth, yet T is still small compared to the gap between the NFBs and the other bands [Fig. 2(a)]. In this case, we may neglect bands other than the NFBs, apply the equipartition scaling for the relaxation times [Eq. (2)], and expand the thermal weighting functions in the formula for the resistivity [Eq. (B1)], giving

$$\frac{\delta^{ij}}{\rho} = \frac{1}{4}\frac{e^2}{(k_B T)^2}\frac{1}{\mathcal{A}}\sum_S c_S v_S^i v_S^j + O\left(\frac{1}{(k_B T)^4}\right). \qquad (3)$$

We thus find a mid-T, $\rho \propto T^2$ scaling regime due entirely to phonon scattering. This is noteworthy since $\rho \propto T^2$ scaling is generally seen as the hallmark of transport dominated by

electron-electron scattering in a Fermi liquid [49,50,52], but the "mid-T" regime generated by NFB phonon scattering has exactly the same T^2 dependence.

IV. ULTRASUBSONIC KINETIC THEORY

In general, determining the relaxation times for Eq. (B1) requires the self-consistent solution of a complicated integral equation: the relaxation time of a state S couples to the relaxation times of all states on the scattering manifold for S, which may have a complicated geometry. However, the "ultrasubsonic (USS) limit" yields transparent analytical results. The USS limit is defined by a generic two-band model, taking both v_F/v_p and the band separation (the maximum energy difference between two points with the same crystal momentum but on opposite bands) to be small parameters [see Fig. 2(b)].

Let S be a state on band b with energy ε, and let $\bar{S}$ denote the state with the same momentum on the opposite band ($\bar{b}$) with energy $\bar{\varepsilon}$. The scattering manifold of the state S will be a loop on band $\bar{b}$ around $\bar{S}$, with radius $|\varepsilon - \bar{\varepsilon}|/(\hbar v_p)$ and the energy variation along the scattering manifold is roughly $(v_F/v_p)|\varepsilon - \bar{\varepsilon}|$ [Fig. 2(b)]. Both quantities are suppressed in the USS limit. This physical picture enables two key approximations. Since the scattering manifold is small and the energy variation along it is negligible, we can approximate $\tau(S') \approx \tau(\bar{S})$ and $\varepsilon' \approx \bar{\varepsilon}$ for states S' along the scattering manifold. The former approximation reduces the self-consistent equation for the relaxation times to a 2×2 matrix equation that can be simply inverted and the latter allows for an analytical solution with transparent, closed-form dependencies on T and μ.

To keep our discussion focused on the key concepts, we will simply state the final answer and present the derivation in full in the Appendixes. For the rest of the paper, to illustrate universal features, we will specialize to the particle-hole-symmetric case, for which the relaxation times are given by

$$\tau_S = \frac{\rho_M \hbar^3 v_p^4}{D^2}\frac{1}{|\varepsilon|^2}\sinh\left(\frac{|\varepsilon|}{k_B T}\right)\frac{1}{X_S^2 - \tilde{X}_S^2}$$
$$\times \left[X_s \frac{\cosh\left(\frac{\varepsilon+\mu}{2k_B T}\right)}{\cosh\left(\frac{\varepsilon-\mu}{2k_B T}\right)} + \tilde{X}_S \frac{\cosh\left(\frac{\varepsilon-\mu}{2k_B T}\right)}{\cosh\left(\frac{\varepsilon+\mu}{2k_B T}\right)} \right], \qquad (4)$$

where ρ_M is the mass density of the system, D is the deformation potential, and the (T, μ)-independent factors X_S and $\tilde{X}_S$ encode wave-function overlap and band geometry data. They are defined explicitly in the Appendixes. Combining the relaxation time formula [Eq. (C8)] with the resistivity formula [Eq. (B1)] gives the master formula for the resistivity of the (particle-hole-symmetric) ultrasubsonic fermion system:

$$\frac{\delta^{ij}}{\rho} = \frac{1}{4}\frac{e^2}{k_B T}\frac{\rho_M \hbar^3 v_p^4}{D^2}\left[\frac{1}{\mathcal{A}}\sum_S \frac{v_S^i v_S^j}{X_S - \tilde{X}_S}\frac{1}{\varepsilon^2}\frac{\sinh\left(\frac{|\varepsilon|}{k_B T}\right)}{\cosh\left(\frac{\varepsilon+\mu}{2k_B T}\right)\cosh\left(\frac{\varepsilon-\mu}{2k_B T}\right)} \right.$$
$$\left. + \frac{1}{2}\sinh\left(\frac{|\mu|}{k_B T}\right)^2 \frac{1}{\mathcal{A}}\sum_S \frac{v_S^i v_S^j X_S}{X_S^2 - \tilde{X}_S^2}\frac{1}{\varepsilon^2}\left[\frac{\sinh\left(\frac{|\varepsilon|}{k_B T}\right)}{\cosh\left(\frac{\varepsilon+\mu}{2k_B T}\right)\cosh\left(\frac{\varepsilon-\mu}{2k_B T}\right)}\right]^3 \right]. \qquad (5)$$
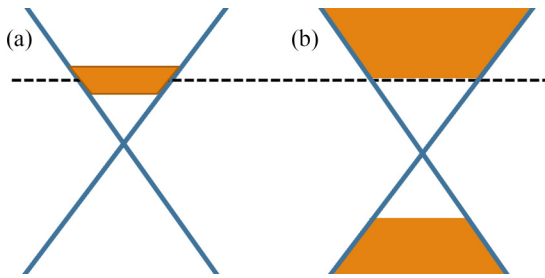
FIG. 3. We depict the difference in the physics of ultra-low-T transport in subsonic and supersonic fermion systems. In each figure, the band structure of the fermions is depicted in blue, and the orange filling indicates the energies of the electrons that contribute meaningfully to transport. The dotted line denotes the Fermi level. In (a), we show the scenario for supersonic fermions, in which only the states in the immediate vicinity of the Fermi surface contribute to transport. In (b), we illustrate the different physics of subsonic fermion scattering, where the states contributing meaningfully to low-T transport are those satisfying $|\varepsilon| > |\mu|$. In this picture, states very far from the Fermi level can contribute much more than states even just barely below it.

In the limit $k_B T \gg |\varepsilon - \bar{\varepsilon}|$, expanding the sinh factor in Eq. (C8) gives the expected $\tau \propto T^{-1}$ scattering rate of the equipartition regime. However, when $k_B T \ll |\varepsilon - \bar{\varepsilon}|$, instead of the usual crossover to a $\tau \propto T^{-4}$ power law, we find an exponential blowup of the relaxation times, in line with a physical picture in which the entire scattering manifold becomes thermally inaccessible.

V. EXTREME LOW-T LIMIT

In Eq. (5), the only T-dependent factor in the Brillouin zone summations is the kernel

$$K(\varepsilon, \mu, T) \equiv \frac{\sinh\left(\frac{|\varepsilon|}{k_B T}\right)}{\cosh\left(\frac{\varepsilon + \mu}{2k_B T}\right)\cosh\left(\frac{\varepsilon - \mu}{2k_B T}\right)}. \tag{6}$$

This factor represents the competition at low T between the divergence of the relaxation times and the thermodynamic suppression of states far from the Fermi level. In the extreme low-T limit, where the sinh and cosh functions blow up exponentially, we simply have

$$K(\varepsilon, \mu, T \to 0) \to 2\Theta[|\varepsilon| - |\mu|]. \tag{7}$$

The thermal kernel K determines which Bloch states meaningfully contribute to transport. Equation (7) suggests that all states with $|\mu| < |\varepsilon|$ contribute equally, while states with $|\mu| > |\varepsilon|$ do not contribute, even though they may be close to the Fermi energy. We emphasize that this is radically different than the usual paradigm, where low-T transport is almost entirely determined by states in the immediate vicinity of the Fermi level. This is depicted in Fig. 3.

Applying the limit (7), the two summations in Eq. (5) are simply T-independent constants ($\mathcal{C}_1, \mathcal{C}_2$), and the extreme low-$T$ expression for the resistivity is

$$\rho \approx \frac{\hbar D^2}{4e^2 \rho_M (\hbar v_p)^4} \frac{k_B T}{\mathcal{C}_1 + \mathcal{C}_2 \sinh[|\mu|/(k_B T)]^2}. \tag{8}$$

From Eq. (8), it is apparent that at the charge-neutrality point ($\mu = 0$), we have purely linear-in-T phonon-induced resistivity down to $T = 0$. On the other hand, when $\mu \neq 0$, then the low-T resistivity is proportional to the factor $\rho \propto \exp[-2|\mu|/(k_B T)]$, and is exponentially suppressed when $k_B T \ll 2|\mu|$, giving a crossover to perfect conductivity. Comparing this with the physics of supersonic fermions, we find

$$k_B T_{\text{crossover}} = 2|\mu| = \frac{v_F}{v_p} k_B T_{\text{BG}}^{\text{trad}}, \tag{9}$$

where $T_{\text{BG}}^{\text{trad}} \equiv 2v_p k_F$ gives the traditional lower bound for the regime of linear-in-T resistivity based on the usual Bloch-Grüneisen paradigm. The crossover temperature is parametrically suppressed by the small parameter v_F/v_p. The ultrasubsonic case is thus expected to host linear-in-T resistivity scaling down to a significantly lower temperature than one would estimate based on intuition from supersonic fermion scattering.

VI. CONCLUDING DISCUSSION

The simple fact that phonon scattering processes in subsonic fermion systems are necessarily interband transitions underlies a robust, linear-in-T scaling of the resistivity down to temperatures far lower than the Bloch-Grüneisen paradigm of supersonic fermion scattering would suggest. This result provides a concrete mechanism for the linear-in-T resistivity over a wide range of temperatures based only on familiar concepts of solid-state physics and the distinct kinematics of NFB systems. In particular, it provides an alternative theoretical explanation for low-T "strange-metal" resistivity scaling in NFB systems.

Our theory also predicts regimes of perfect conductivity and $\rho \propto T^2$ scaling which compete with the $\rho \propto T$ regime, which are not commonly associated with phonon physics. Thus, low-T $\rho \propto T$, $\rho \propto T^2$, and perfect conductivity regimes may all arise in NFB systems from the same universal phonon-scattering physics, providing a possible explanation for these reported observations in MATBLG [42]. Further, there has been some disagreement in the literature about where SC can be found in the MATBLG phase diagram, with some groups claiming to find regions of SC (e.g., [13]) that have not been reported by other groups [8,11]. Especially since the Meissner effect cannot be used as a verification of SC, a phonon mechanism that can produce perfect conductivity mimicking SC could explain these sporadic SC observations.

Without particle-hole (PH) symmetry the competition between linear-in-T resistivity and perfect conductivity depends sensitively on the band structure details. Since the true interaction-renormalized MATBLG band structure is unknown, we refrain from a detailed consideration of the specifics of the Bistritzer-MacDonald (BM) model and keep our focus on general considerations of subsonic fermions transport. However, we discuss the BM model more quantitatively in the Appendixes.

Future work should investigate the roles of strain, disorder, and interaction-renormalization effects on this mechanism. In particular, studying disorder is important: while graphene-based NFB systems are remarkably disorder free, all systems

contain *some* disorder, and even trace amounts of disorder could play an important role in cutting the proposed exponential growth of the relaxation times. In particular, we expect that trace disorder could render states far from the Fermi surface (FS) inert and define an energy window about the FS determining which states contribute meaningfully to transport. On one hand, this could produce interesting corrections to our results dependent on the interplay of the disorder strength and the band geometry near the FS. On the other, by killing the contributions from the far-from-FS states, disorder could in fact *stabilize* the linear-in-T resistivity regime in the non-PH-symmetric case. Indeed, if subsonic fermion transport is sensitive to trace amounts of disorder, then this could help explain the huge sample-to-sample variation observed in experiments on MATBLG systems known to have extremely low disorder. However, quantitative inclusion of other effects in the theory beyond the BM model such as interaction, strain, and disorder should await future MATBLG experiments reaching a stronger consensus on transport phenomena. At this stage, when MATBLG transport experiments themselves show considerable sample to sample variations with little quantitative agreement, our excellent qualitative agreement with MATBLG transport is all that we can aim for.

APPENDIX A: MICROSCOPIC MODEL OF PHONON COUPLING

In this Appendix we give an an explicit microscopic model for the electron-phonon coupling of a subsonic fermion system. We will use the formalism of a layered graphene system. We consider a general, subsonic two-band fermion system coupled via the standard deformation potential [46,49,52] to longitudinal acoustic phonons in the Debye approximation. Our model is described by the Hamiltonian

$$H = H^e + H^{ph} + H^{e\text{-}ph}, \tag{A1}$$

$$H^{ph} = \sum_{l,\mathbf{q}} \hbar\omega_{\mathbf{q}} a_{l,\mathbf{q}}^\dagger a_{l,\mathbf{q}}, \tag{A2}$$

$$H^{e\text{-}ph} = \sqrt{\frac{D^2\hbar}{2\rho_M \mathcal{A}}} \sum_{l,\mathbf{q}} \frac{\hat{n}_{\mathbf{q},l}}{\sqrt{\omega_{\mathbf{q}}}} (-i\mathbf{q} \cdot \hat{e}_{\mathbf{q}})(a_{\mathbf{q},l} + a_{-\mathbf{q},l}^\dagger). \tag{A3}$$

Above, $\mathcal{A}$ is the area of the system, ρ_M is the mass density of the system, D is the deformation potential, $\hat{e}_{\mathbf{q}}$ is the displacement unit vector of the phonon, and $\omega_{\mathbf{q}}$ is the phonon dispersion. The summation over the vector $\mathbf{q}$ runs over the Brillouin zone, and l is a layer index, making our formalism tailored to layered graphene systems. (In a nonlayered system, the l summation is trivial.) Finally, the electron density operator is

$$\hat{n}_{\mathbf{q},l} \equiv \sum_{\mathbf{k}} c_{(\mathbf{k}+\mathbf{q}),l}^\dagger c_{\mathbf{k},l}. \tag{A4}$$

where $c_{\mathbf{k}}^\dagger \equiv c_{s,\xi,\sigma,l,\mathbf{k}}^\dagger$ creates an electron with momentum $\mathbf{k}$, spin s, valley ξ, sublattice σ, and layer l. Summations over the unwritten indices s, ξ, and σ are implicit in Eq. (A4). We emphasize that none of the physics described in this paper depend on the degenerate spin and valley degrees of freedom. We use the Debye approximation $\omega_{\mathbf{q}} \approx v_p|\mathbf{q}|$, where v_p is the phonon (or sound) velocity of graphene. (Since our focus is on the extreme low-T limit, the Debye approximation is particularly justified.) The standard values of the above parameters for monolayer graphene are $D = 25\text{eV}$, $\rho_M = 7.6 \times 10^{-8}$ g/cm^2, and $v_p = 2.0 \times 10^6$ cm/s, [43,46,51,53]. Using these values in the theory gives accurate quantitative predictions for transport in many layered graphene systems [43,45,47].

The single-particle electron Hamiltonian H^e determines the electronic band structure, which we do not specify in order to preserve generality. However, we will consider a two-band system and assume both that $v_F \ll v_p$ and that the separation between the bands is small. We call the limit in which both these assumptions are valid the "ultrasubsonic" (USS) limit.

APPENDIX B: BOLTZMANN KINETIC THEORY DETAILS

Here we provide additional details on the fundamental equations of the Boltzmann kinetic theory framework for longitudinal acoustic phonon-limited transport. As stated in the main text [Eq. (1)], the resistivity of the system follows from the relaxation times via

$$\frac{\delta^{ij}}{\rho} = \frac{1}{4}\frac{e^2}{k_B T}\frac{1}{\mathcal{A}} \sum_S \frac{\tau_S v_S^i v_S^j}{\cosh\left(\frac{\varepsilon-\mu}{2k_B T}\right)^2}. \tag{B1}$$

The relaxation times are determined from a self-consistent integral equation, derived from the Boltzmann equation. In the case of longitudinal acoustic phonons, in the Debye approximation, which couple to the fermions via the deformation potential, this takes the form [43,45–47,49,51]

$$\frac{\pi D^2}{\hbar\rho_M v_p^2}\frac{1}{\mathcal{A}} \sum_{S'} \tilde{\Delta}_{S,S'}\mathcal{C}_{S,S'}\mathcal{F}_{S,S'}^{\mu,T}\left[\tau_S - \tau_{S'}\frac{\mathbf{v}_{S'} \cdot \mathbf{v}_S}{v_s^2}\right] = 1. \tag{B2}$$

Above, ρ_M is the mass density of the system, D is the deformation potential, and v_p is the phonon velocity. In a layered graphene system, we note that the summation over states S in Eqs. (B1) and (B2) includes a fourfold degeneracy over spin and valley degrees of freedom. The function $\tilde{\Delta}_{S,S'}$ enforces the conservation of energy and momentum and defines the scattering manifold:

$$\tilde{\Delta}_{S,S'} \equiv \delta_{s,s'}\delta_{\xi,\xi'}\Delta_{S,S'} \equiv \delta_{s,s'}\delta_{\xi,\xi'}\delta(|\varepsilon' - \varepsilon| - \hbar v_p|\mathbf{k}' - \mathbf{k}|). \tag{B3}$$

Note that the energy-momentum conservation assumes the Debye dispersion for the phonons. The function

$$\mathcal{F}_{S,S'}^{\mu,T} \equiv \frac{|\varepsilon' - \varepsilon|}{2}\frac{1}{\sinh\left[\frac{|\varepsilon'-\varepsilon|}{2k_B T}\right]}\frac{\cosh\left[\frac{\varepsilon-\mu}{2k_B T}\right]}{\cosh\left[\frac{\varepsilon'-\mu}{2k_B T}\right]} \tag{B4}$$

encodes all the thermodynamics, including the occupation data for the fermions and phonons and all dependence on μ and T. Finally, $\mathcal{C}_{S,S'}$ are "matrix elements" encoding geometric

wave-function overlap data [43,45–47], and are given by

$$\mathcal{C}_{S,S'} \equiv \sum_l \left| \langle S' | \hat{n}_{l,\mathbf{q}} | S \rangle \right|^2. \tag{B5}$$

In $\mathcal{C}_{S,S'}$, the wave-function overlap is given by

$$\langle S' | \hat{n}_{l,\mathbf{q}} | S \rangle = \sum_{\sigma, \mathbf{G}, \mathbf{G}'} V^*_{b', \mathbf{k}'; \sigma, l, \mathbf{G}} V_{b, \mathbf{k}; \sigma, l, \mathbf{G}'} \delta_{\mathbf{k}' + \mathbf{G}', \mathbf{k} + \mathbf{G} + \mathbf{q}}, \tag{B6}$$

where $\mathbf{k}, \mathbf{k}'$ take values in the (moiré) Brillouin zone and $\mathbf{G}, \mathbf{G}'$ take values on the (moiré) reciprocal lattice. The matrix elements V define the (moiré) Bloch wave functions that are eigenstates of the Hamiltonian:

$$\tilde{c}^\dagger_{s, \xi, b, \mathbf{k}} = \sum_{\sigma, l, \mathbf{G}} V_{b, \mathbf{k}; \sigma, l, \mathbf{G}} \, c^\dagger_{s, \xi, \sigma, l, \mathbf{k} + \mathbf{G}}, \tag{B7}$$

such that

$$H^e = \sum_{s, \xi, b, \mathbf{k}} \varepsilon_{s, \xi, b, \mathbf{k}} \tilde{c}^\dagger_{s, \xi, b, \mathbf{k}} \tilde{c}_{s, \xi, b, \mathbf{k}}. \tag{B8}$$

On a finite-momentum grid, Eq. (B2) is a matrix inversion problem that can be solved for the relaxation times τ_S. Equation (B1) then gives the resistivity.

APPENDIX C: ULTRASUBSONIC TRANSPORT THEORY: DERIVATION DETAILS

We give the details for the derivation of the main results of ultrasubsonic (USS) transport theory [Eqs. (4) and (5) in the main text] and state the general version of the particle-hole-symmetric result given in those equations. As discussed in the main text, the technical advantage of the USS limit is the justification of the approximations $\mathcal{F}^{\mu, T}(S, S') \approx \mathcal{F}^{\mu, T}(S, \bar{S})$ and $\tau(S') \approx \tau(\bar{S})$ which replace the relaxation times and the thermal occupancy function at points along the scattering manifold (S') by their values at the complement point ($\bar{S}$). Applying these simplifications to Eq. (B2), we have

$$1 = \frac{\pi D^2}{\hbar \rho_M v_p^2} \mathcal{F}^{\mu, T}_{S, \bar{S}} \left(\tau_S \left[\frac{1}{\mathcal{A}} \sum_{S'} \tilde{\Delta}_{S, S'} \mathcal{C}_{S, S'} \right] - \tau_{\bar{S}} \left[\frac{1}{|\mathbf{v}_S|} \frac{1}{\mathcal{A}} \sum_{S'} \tilde{\Delta}_{S, S'} \mathcal{C}_{S, S'} |\mathbf{v}_{S'}| \cos \theta_{\mathbf{v}} \right] \right) \tag{C1}$$

$$= \frac{\pi D^2}{\hbar \rho_M v_p^2} \mathcal{F}^{\mu, T}_{S, \bar{S}} \left(\tau_S \left[\int \frac{d^2 \mathbf{k}'}{(2\pi)^2} \Delta_{S, S'} \mathcal{C}_{S, S'} \right] - \tau_{\bar{S}} \left[\frac{1}{|\mathbf{v}_S|} \int \frac{d^2 \mathbf{k}'}{(2\pi)^2} \Delta_{S, S'} \mathcal{C}_{S, S'} |\mathbf{v}_{S'}| \cos \theta_{\mathbf{v}} \right] \right) \tag{C2}$$

$$\equiv \frac{D^2}{2 \rho_M \hbar^3 v_p^4} |\varepsilon - \bar{\varepsilon}| \mathcal{F}^{\mu, T}_{S, \bar{S}} [X_S \tau_S - \tilde{X}_S \tau_{\bar{S}}], \tag{C3}$$

where in the second line we have taken the thermodynamic limit (continuum limit in momentum space) and in the last line we have defined the (T, μ)-independent factors

$$X_S \equiv \frac{2\pi (\hbar v_p)^2}{|\varepsilon - \bar{\varepsilon}|} \int \frac{d^2 \mathbf{k}'}{(2\pi)^2} \Delta_{S, S'} \mathcal{C}_{S, S'}, \tag{C4}$$

$$\tilde{X}_S \equiv \frac{2\pi (\hbar v_p)^2}{|\varepsilon - \bar{\varepsilon}|} \int \frac{d^2 \mathbf{k}'}{(2\pi)^2} \Delta_{S, S'} \mathcal{C}_{S, S'} \frac{v_{s'}}{v_s} \cos \theta_{v, v'}, \tag{C5}$$

which encode wave-function overlap and band geometry data. To motivate the prefactors in the definitions above, we note that if we approximate the scattering manifold as a circle around $\bar{S}$, we simply have

$$X_S \approx \frac{2\pi (\hbar v_p)^2}{|\varepsilon - \bar{\varepsilon}|} \int \frac{dq \, q}{(2\pi)} \delta[|\varepsilon - \bar{\varepsilon}| - \hbar v_p q] \int_0^{2\pi} \frac{d\phi}{(2\pi)} \mathcal{C}_{S, S'}$$

$$= \int_0^{2\pi} \frac{d\phi}{(2\pi)} \mathcal{C}_{S, S'}. \tag{C6}$$

We emphasize that $X_S, \tilde{X}_S$ depend on the state index S via the wave function and the local geometry of the bands in the vicinity of S. Pairing Eq. (C3) with the corresponding one for the state $\bar{S}$ gives a 2×2 matrix equation:

$$\frac{D^2}{2 \rho_M \hbar^3 v_p^4} |\varepsilon - \bar{\varepsilon}| \begin{bmatrix} \mathcal{F}^{\mu, T}_{S, \bar{S}} X_S & -\mathcal{F}^{\mu, T}_{S, \bar{S}} \tilde{X}_S \\ -\mathcal{F}^{\mu, T}_{\bar{S}, S} \tilde{X}_{\bar{S}} & \mathcal{F}^{\mu, T}_{\bar{S}, S} X_{\bar{S}} \end{bmatrix} \begin{bmatrix} \tau_S \\ \tau_{\bar{S}} \end{bmatrix} = \begin{bmatrix} 1 \\ 1 \end{bmatrix}. \tag{C7}$$

Simply inverting the 2×2 matrix, using the full form of $\mathcal{F}^{\mu, T}_{S, \bar{S}}$ from Eq. (B4) and simplifying gives the general solution for the relaxation time of a USS system,

$$\tau_S = \frac{2 \rho_M \hbar^3 v_p^4}{D^2} \frac{2}{|\varepsilon - \bar{\varepsilon}|^2} \sinh\left(\frac{|\varepsilon - \bar{\varepsilon}|}{2 k_B T} \right) \frac{1}{X_S X_{\bar{S}} - \tilde{X}_S \tilde{X}_{\bar{S}}} \left[X_{\bar{S}} \frac{\cosh\left(\frac{\bar{\varepsilon} - \mu}{2 k_B T} \right)}{\cosh\left(\frac{\varepsilon - \mu}{2 k_B T} \right)} + \tilde{X}_S \frac{\cosh\left(\frac{\varepsilon - \mu}{2 k_B T} \right)}{\cosh\left(\frac{\bar{\varepsilon} - \mu}{2 k_B T} \right)} \right]. \tag{C8}$$

Combining the relaxation time formula [Eq. (C8)] with the resistivity formula [Eqs. (1) and (B1)] gives the master formula for the resistivity of the ultrasubsonic fermion system:

$$
\frac{\delta^{ij}}{\rho} = \frac{e^2 \rho_M (\hbar v_p)^4}{\hbar D^2 k_B T} \frac{1}{\mathcal{A}} \sum_{\varepsilon_S > 0} \frac{1}{|\varepsilon - \bar{\varepsilon}|^2} \frac{\sinh\left(\frac{|\varepsilon - \bar{\varepsilon}|}{2 k_B T}\right)}{\cosh\left(\frac{\bar{\varepsilon} - \mu}{2 k_B T}\right) \cosh\left(\frac{\varepsilon - \mu}{2 k_B T}\right)} \frac{1}{X_S X_{\bar{S}} - \tilde{X}_S \tilde{X}_{\bar{S}}} \left\{ \begin{array}{l} (\tilde{X}_S + X_{\bar{S}}) v_S^i v_S^j + (\tilde{X}_{\bar{S}} + X_S) v_{\bar{S}}^i v_{\bar{S}}^j \\[8pt] + \sinh\left(\frac{\bar{\varepsilon} - \varepsilon}{2 k_B T}\right) \sinh\left(\frac{\bar{\varepsilon} + \varepsilon - 2\mu}{2 k_B T}\right) \\[8pt] \times \left[\dfrac{X_{\bar{S}} v_S^i v_S^j}{\cosh\left(\frac{\varepsilon - \mu}{2 k_B T}\right)^2} - \dfrac{X_S v_{\bar{S}}^i v_{\bar{S}}^j}{\cosh\left(\frac{\bar{\varepsilon} - \mu}{2 k_B T}\right)^2} \right] \end{array} \right\}.
\tag{C9}
$$

We emphasize that the complexity of the particle-hole-symmetry-breaking terms in the brackets of Eq. (C9) significantly complicated the competition between the regimes of linear-in-T resistivity and perfect conductivity discussed in the main text. These terms depend sensitively on band structure details. To extract easily comprehensible general features of USS transport, in the main text we focus on the particle-hole-symmetric limit. In this case, enforcing particle-hole symmetry on our results [Eqs. (C8) and (C9)] simply amounts to setting $\bar{\varepsilon} = -\varepsilon$, $X_{\bar{S}} = X_S$, and $\tilde{X}_{\bar{S}} = \tilde{X}_S$. Making these substitutions in Eqs. (C8) and (C9) yields Eqs. (4) and (5) in the main text.

Finally, as noted in the main text, the high-T limit ($k_B T \gg |\varepsilon - \bar{\varepsilon}|$) gives the expected $\tau \propto T^{-1}$ scattering rate of the equipartition regime [Eq. (2)]. Taking this limit in Eq. (C8), we see that for USS fermions, the constants c_S are given explicitly by

$$
c_S = \frac{2 \rho_M (\hbar v_p)^4}{\hbar D^2} \frac{1}{|\varepsilon - \bar{\varepsilon}|} \frac{X_{\bar{S}} + \tilde{X}_S}{X_S X_{\bar{S}} - \tilde{X}_S \tilde{X}_{\bar{S}}}.
\tag{C10}
$$

In the PH-symmetric limit we have

$$
c_S = \frac{\rho_M (\hbar v_p)^4}{\hbar D^2} \frac{1}{|\varepsilon|} \frac{1}{X_S - \tilde{X}_S}.
\tag{C11}
$$

APPENDIX D: HIERARCHY OF APPROXIMATIONS IN ULTRASUBSONIC LIMIT

We formalize the hierarchy of simplifications that follow from the ultrasubsonic (USS) limit. The USS limit is defined as the limit of both the small dimensionless ration of velocities v_F / v_s and small separation between the two bands of the electronic band structure. By small band separation, we specifically mean that

$$
\frac{1}{\hbar v_p} |\varepsilon_S - \varepsilon_{\bar{S}}| \ll 1
\tag{D1}
$$

for all (moiré) Bloch states S (with complement state $\bar{S}$).

The USS limit allows us to make a series of approximations that give analytical, closed-form solutions to the Boltzmann transport equation [Eq. (B2)]. The various approximations are as follows:

(1) "USS 1": $\tau(S') \approx \tau(\bar{S})$ along the scattering manifold.

(2) "USS 2": In addition to USS 1, we further assume that $\mathcal{F}_{S,S'}^{\mu,T} \approx \mathcal{F}_{S,\bar{S}}^{\mu,T}$ along the scattering manifold.

(3) "USS 3": In addition to USS 1 and USS 2, we also approximate the scattering manifold as a small circle around the point $\bar{S}$, as in Eq. (C6).

We justify USS 1 by noting that the small band separation [Eq. (D1)] means that the scattering manifold for state S is a small loop centered around $\bar{S}$ on the opposite band. To see this geometrically, see Fig. 2(b) in the main text. Since the wave functions, energies, and Fermi velocities are continuous along the scattering manifold we expect the relaxation times to also be continuous. (If the scattering manifold included a Dirac point, the wave function would not necessarily be continuous. However, for subsonic fermions, this is ruled out by geometry. It is impossible to scatter to a subsonic Dirac point.) The small scattering manifold then allows USS 1. We note that USS 1 is the key technical step of this paper since it is the simplification that allows the reduction of the integral equation in Eq. (B2) to a 2×2 matrix equation. We emphasize that it is similar in spirit to the "quasielastic" approximation used throughout the standard treatments of transport in graphene [43,44,46,48,51], which assumes that the relaxation time of a state S is identical to the relaxation times on its own scattering manifold. The quasielastic approximation is natural for a strongly supersonic fermion system, like graphene or traditional metal, and in those systems reduces the Boltzmann transport integral equation to an algebraic equation that can be solved in closed form. The USS 1 approximation is the natural analog for a strongly subsonic system. (We emphasize that the quasielastic approximation for supersonic fermion systems requires additional assumptions, usually isotropy, which are not required for the USS 1 approximation in the USS limit.)

USS 2 is justified similarly by estimating that the total energy variation along the scattering manifold is

$$
\Delta \varepsilon \approx \frac{v_F}{v_p} |\varepsilon_S - \varepsilon_{\bar{S}}|,
\tag{D2}
$$

which is parametrically suppressed by the USS limit. Since the thermodynamic occupancy function $\mathcal{F}_{S,S'}^{\mu,T}$ depends on S, S' only through their energies, USS 2 is very natural. We note that at a technical level, USS 2 is *not* required in order to reduce the Boltzmann equation to a matrix equation. However, USS 2 allows us to factor out all temperature and doping dependencies from the integral equation in Eq. (B2) and makes the temperature and doping dependencies of the relaxation times and resistivity transparent. If one wants to avoid USS
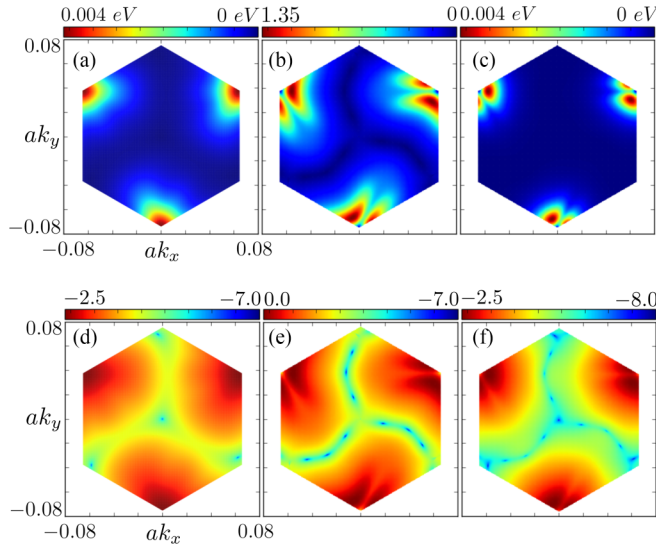
FIG. 4. We demonstrate the extent of the applicability of the ultrasubsonic scattering theory to MATBLG by providing numerical heat maps of some crucial quantities, calculated for the Bistritzer-MacDonald model for the noninteracting band structure of MATBLG. We use the standard BM Hamiltonian with the interlayer hopping parameters $\omega_0 = 90$ meV, $\omega_1 = 117$ meV, and the bare graphene Dirac cone velocity $v_F = 10^6$ m/s, which places the "magic angle" at $\theta = 1.025°$. We take $v_p = 2 \times 10^4$ m/s, consistent with phonon speeds in single-layer graphene [43]. In the left column [(a) and (d)], we depict the energy difference between the two NFBs, $|\varepsilon_S - \varepsilon_{\bar{S}}|$. We note that it is very small except for a single peak. In the center [(c) and (e)], we calculate the dimensionless ratio v_F/v_p. We see that the majority of the band is strongly subsonic, though there are supersonic Bloch states near the peak. Finally, in the right column [(c) and (f)], we plot the product of these two quantities, which is the energy scale justifying the USS approximations that enable our theory. For each quantity, we plot the data in a linear scale on the top row (a)–(c) and a logarithm scale on the bottom row (d)–(f).

2, a generalized definition of $X_S, \tilde{X}_S$ that incorporates temperature dependence could be used.

Finally, we note that we do not use USS 3 anywhere in the main text. It is useful if one wants to approximate $X_S, \tilde{X}_S$ for a specific model.

APPENDIX E: ULTRASUBSONIC DIRAC CONE

As a concrete example, we apply our results to the ultrasubsonic Dirac cone, where the simple band structure can be used to to evaluate the formulas explicitly. We must evaluate X_S and $\tilde{X}_S$. By symmetry, X_S and $\tilde{X}_S$ will only depend on the state S via the energy ε, though we will see that in the case of the Dirac cone they are also ε independent. We let $r \equiv v_F/v_p$.

For the subsonic Dirac cone, we have $\cos\theta_v = -\cos\theta$, where θ is the momentum angle and

$$\mathcal{C}_{S,S'} = \frac{1}{2}(1 - \cos\theta). \quad (E1)$$

Analyzing the kinematics of phonon scattering on the Dirac cone, we see that the scattering manifold for the interband transitions in the subsonic Dirac cone is an ellipse parametrized by the momentum transfer vector

$$q(\phi) = \frac{2rk}{1 - r^2}(1 + r\cos\phi), \quad (E2)$$

where ϕ is the angle between the momentum of the initial fermion state and the phonon state. Some trigonometry gives the momentum angle (θ) in terms of ϕ:

$$\cos\theta = 1 - \frac{2r^2\sin^2\phi}{1 + r^2 + 2r\cos\phi}. \quad (E3)$$

We may then evaluate

$$X_S(r) = \frac{2\pi(\hbar v_p)^2}{|\varepsilon - \bar{\varepsilon}|}\int\frac{dq\,q}{(2\pi)}\int_0^{2\pi}\frac{d\phi}{(2\pi)}\delta[|\varepsilon - \varepsilon'| - \hbar v_p q]\mathcal{C}_{S,S'} \quad (E4)$$

$$= \frac{\hbar v_p}{4|\varepsilon|}\int_0^{2\pi}\frac{d\phi}{2\pi}q(\phi)\big(1 - \cos[\theta(\phi)]\big) \quad (E5)$$

$$= \frac{1}{2}\int_0^{2\pi}\frac{d\phi}{2\pi}\frac{1 + r\cos\phi}{1 - r^2}\left[\frac{2r^2\sin^2\phi}{1 + r^2 + 2r\cos\phi}\right]. \quad (E6)$$

We note that Eq. (E6) is an exact evaluation of X_S that does not make use of the approximation "USS 3," and we point out that the final answer has no dependence on the state S. Similarly,

$$\tilde{X}_S(r) \approx \frac{-1}{2}\int_0^{2\pi}\frac{d\phi}{2\pi}\frac{1 + r\cos\phi}{1 - r^2}\left[\frac{2r^2\sin^2\phi}{1 + r^2 + 2r\cos\phi}\right]$$

$$\times\left[1 - \frac{2r^2\sin^2\phi}{1 + r^2 + 2r\cos\phi}\right] \quad (E7)$$

$$= -X(r) + \frac{1}{2}\int_0^{2\pi}\frac{d\phi}{2\pi}\frac{1 + r\cos\phi}{1 - r^2}$$

$$\times\left[\frac{2r^2\sin^2\phi}{1 + r^2 + 2r\cos\phi}\right]^2. \quad (E8)$$

Like Eq. (E6) for $X(r)$, Eq. (E8) gives an exact expression for $\tilde{X}_S$ and shows that there is no dependence on the initial state S.

Working to leading order in v_F/v_p we simply have

$$X = \frac{1}{2}\left(\frac{v_F}{v_p}\right)^2, \quad \tilde{X} = \frac{3}{4}\left(\frac{v_F}{v_p}\right)^4 - X. \quad (E9)$$

The above results show that

$$\frac{1}{X_S - \tilde{X}_S} \approx \frac{1}{r^2}\frac{4}{4 - 3r^2} = \left(\frac{v_p}{v_F}\right)^2\frac{4v_p^2}{4v_p^2 - 3v_F^2}, \quad (E10)$$

$$\frac{X_S}{X_S^2 - \tilde{X}_S^2} \approx \frac{2}{3r^4}\frac{4}{4 - 3r^2} = \frac{2}{3}\left(\frac{v_p}{v_F}\right)^4\frac{4v_p^2}{4v_p^2 - 3v_F^2}. \quad (E11)$$

Applying Eqs. (E10) and (E11) to the PH-symmetric resistivity formula [Eq. (5)] and using the Dirac cone band structure gives a concrete formula for the resistivity of the

USS Dirac cone:

$$\frac{1}{\rho} \approx \frac{1}{k_B T}\frac{2}{\pi}\frac{e^2 \rho_M \hbar v_p^4}{D^2}\left(\frac{v_p}{v_F}\right)^2 \frac{v_p^2}{4v_p^2 - 3v_F^2}\left[\int_0^\Lambda \frac{d\varepsilon}{\varepsilon}\frac{\sinh\left(\frac{\varepsilon}{k_B T}\right)}{\cosh\left(\frac{\varepsilon+\mu}{2k_B T}\right)\cosh\left(\frac{\varepsilon-\mu}{2k_B T}\right)} + \frac{1}{3}\left(\frac{v_p}{v_F}\right)^2 \sinh\left(\frac{|\mu|}{k_B T}\right)^2 \int_0^\Lambda \frac{d\varepsilon}{\varepsilon}\left[\frac{\sinh\left(\frac{\varepsilon}{k_B T}\right)}{\cosh\left(\frac{\varepsilon+\mu}{2k_B T}\right)\cosh\left(\frac{\varepsilon-\mu}{2k_B T}\right)}\right]^3\right]. \tag{E12}$$

Specializing to the $\mu = 0$ case, we find

$$\rho \approx \frac{\pi k_B T D^2}{e^2 \rho_M \hbar v_p^4}\frac{v_F^2}{v_p^2}\left(1 - \frac{3}{4}\frac{v_F^2}{v_p^2}\right)\ln\left[\frac{\Lambda}{k_B T}\right]^{-1} \tag{E13}$$

which gives a purely linear-in-T resistivity, up to cutoff-dependent logarithmic corrections. Away from $\mu = 0$ but in the extreme low-T limit, we may make the simplification from Eq. (9) of the main text. This gives

$$\rho \approx \frac{v_F^4}{v_p^8}\frac{\pi D^2 k_B T}{e^2 \rho_M \hbar}\frac{1}{\ln(\Lambda/|\mu|)}e^{-2|\mu|/(k_B T)} \tag{E14}$$

in the $r, T \to 0$ asymptote. The final resistivity formulas for the USS Dirac cone demonstrate the general features of USS transport, showing robust linear-in-T resistivity partially generated by states far from the Fermi level and a crossover to perfect conductivity with exponentially suppressed scattering when $k_B T \ll 2|\mu|$. We note that the prefactor contains nontrivial power-law dependencies on the velocities v_F and v_p that could prove useful for experimental probes of USS transport physics in systems for which the Dirac cone is a useful model.

APPENDIX F: ULTRASUBSONIC FERMIONS IN MATBLG

We close with a more quantitative discussion of the applicability of USS transport theory to MATBLG in particular. In Fig. 4, using the Bistritzer-MacDonald (BM) model for the noninteracting band structure of MATBLG [3], we give numerical heat maps of the interband spacing, the ratio v_F/v_p, and the product of these quantities for the NFBs. It is clear from these figures that the vast majority of the Bloch states in the moiré Brillouin zone are very well captured by the subsonic limit, with energy spacing below 0.0005 eV and $v_F/v_p < 0.01$. For some states, these values approach zero. We further emphasize that while these systems do have significant twist-angle disorder, they are almost entirely free from impurities that would cause elastic scattering, indicating that transport is indeed likely phonon dominated.

Even in the noninteracting BM model, the NFBs are not entirely subsonic: there is a small "high"-energy hump in the dispersion at the Γ point, characterized by energy separations a large as 0.004 eV and v_F/v_p as large as 1.35. The coexistence of subsonic and supersonic states in the band would need to be taken into account to correctly apply USS scattering theory to the BM band structure in a quantitative way. For example, some subsonic states near the high-energy region may still experience intraband scattering. Even after significant band renormalization, it is possible that large portions of the NFB are well captured by the ultrasubsonic limit and exhibit the related low-T transport phenomena. Indeed, there is evidence that interaction-driven band renormalizations further flatten the band [54].

[1] A. K. Geim and I. V. Grigorieva, Nature (London) **499**, 419 (2013).

[2] K. S. Novoselov, E. McCann, S. V. Morozov, V. I. Fal'ko, M. I. Katsnelson, U. Zeitler, D. Jiang, F. Schedin, and A. K. Geim, Nat. Phys. **2**, 177 (2006).

[3] R. Bistritzer and A. H. MacDonald, Proc. Natl. Acad. Sci. USA **108**, 12233 (2011).

[4] E. S. Morell, J. D. Correa, P. Vargas, M. Pacheco, and Z. Barticevic, Phys. Rev. B **82**, 121407(R) (2010).

[5] X. Li, F. Wu, and A. H. MacDonald, arXiv:1907.12338.

[6] K. Kim, A. DaSilva, S. Huang, B. Fallahazad, S. Larentis, T. Taniguchi, K. Watanabe, B. J. LeRoy, A. H. MacDonald, and E. Tutuc, Proc. Natl. Acad. Sci. USA **114**, 3364 (2017).

[7] Y. Cao, V. Fatemi, A. Demir, S. Fang, S. L. Tomarken, J. Y. Luo, J. D. Sanchez-Yamagishi, K. Watanabe, T. Taniguchi, E. Kaxiras et al., Nature (London) **556**, 80 (2018).

[8] Y. Cao, V. Fatemi, S. Fang, K. Watanabe, T. Taniguchi, E. Kaxiras, and P. Jarillo-Herrero, Nature (London) **556**, 43 (2018).

[9] Y. Cao, D. Chowdhury, D. Rodan-Legrain, O. Rubies-Bigorda, K. Watanabe, T. Taniguchi, T. Senthil, and P. Jarillo-Herrero, Phys. Rev. Lett. **124**, 076801 (2020).

[10] Y. Cao, J. M. Park, K. Watanabe, T. Taniguchi, and P. Jarillo-Herrero, Nature (London) **595**, 526 (2021).

[11] M. Yankowitz, S. Chen, H. Polshyn, Y. Zhang, K. Watanabe, T. Taniguchi, D. Graf, A. F. Young, and C. R. Dean, Science **363**, 1059 (2019).

[12] A. Kerelsky, L. J. McGilly, D. M. Kennes, L. Xian, M. Yankowitz, S. Chen, K. Watanabe, T. Taniguchi, J. Hone, C. Dean et al., Nature (London) **572**, 95 (2019).

[13] X. Lu, P. Stepanov, W. Yang, M. Xie, M. A. Aamir, I. Das, C. Urgell, K. Watanabe, T. Taniguchi, G. Zhang et al., Nature (London) **574**, 653 (2019).

[14] P. Stepanov, I. Das, X. Lu, A. Fahimniya, K. Watanabe, T. Taniguchi, F. H. Koppens, J. Lischner, L. Levitov, and D. K. Efetov, Nature (London) **583**, 375 (2020).

[15] A. L. Sharpe, E. J. Fox, A. W. Barnard, J. Finney, K. Watanabe, T. Taniguchi, M. A. Kastner, and D. Goldhaber-Gordon, Science **365**, 605 (2019).

[16] G. Chen, A. L. Sharpe, E. J. Fox, Y.-H. Zhang, S. Wang, L. Jiang, B. Lyu, H. Li, K. Watanabe, T. Taniguchi *et al.*, Nature (London) **579**, 56 (2020).

[17] A. Rozen, J. M. Park, U. Zondiner, Y. Cao, D. Rodan-Legrain, T. Taniguchi, K. Watanabe, Y. Oreg, A. Stern, E. Berg *et al.*, Nature (London) **592**, 214 (2021).

[18] H. Zhou, L. Holleis, Y. Saito, L. Cohen, W. Huynh, C. L. Patterson, F. Yang, T. Taniguchi, K. Watanabe, and A. F. Young, Science **375**, 774 (2022).

[19] H. Zhou, T. Xie, T. Taniguchi, K. Watanabe, and A. F. Young, Nature (London) **598**, 434 (2021).

[20] H. Zhou, T. Xie, A. Ghazaryan, T. Holder, J. R. Ehrets, E. M. Spanton, T. Taniguchi, K. Watanabe, E. Berg, M. Serbyn *et al.*, Nature (London) **598**, 429 (2021).

[21] M. Serlin, C. L. Tschirhart, H. Polshyn, Y. Zhang, J. Zhu, K. Watanabe, T. Taniguchi, L. Balents, and A. F. Young, Science **367**, 900 (2020).

[22] F. Wu, A. MacDonald, and I. Martin, Phys. Rev. Lett. **121**, 257001 (2018).

[23] F. Wu, T. Lovorn, E. Tutuc, I. Martin, and A. H. MacDonald, Phys. Rev. Lett. **122**, 086402 (2019).

[24] C. L. Tschirhart, E. Redekop, L. Li, T. Li, S. Jiang, T. Arp, O. Sheekey, T. Taniguchi, K. Watanabe, K. F. Mak *et al.*, arXiv:2205.02823.

[25] H. Polshyn, J. Zhu, M. A. Kumar, Y. Zhang, F. Yang, C. L. Tschirhart, M. Serlin, K. Watanabe, T. Taniguchi, A. H. MacDonald *et al.*, Nature (London) **588**, 66 (2020).

[26] A. Jaoui, I. Das, G. Di Battista, J. Díez-Mérida, X. Lu, K. Watanabe, T. Taniguchi, H. Ishizuka, L. Levitov, and D. K. Efetov, arXiv:2108.07753.

[27] H. Polshyn, M. Yankowitz, S. Chen, Y. Zhang, K. Watanabe, T. Taniguchi, C. R. Dean, and A. F. Young, Nat. Phys. **15**, 1011 (2019).

[28] B. Sarma, S. Borah, A. Kani, and J. Twamley, Phys. Rev. Res. **4**, L042038 (2022).

[29] Y. Zhang, R. Polski, A. Thomson, É. Lantagne-Hurtubise, C. Lewandowski, H. Zhou, K. Watanabe, T. Taniguchi, J. Alicea, and S. Nadj-Perge, Nature (London) **613**, 268 (2023).

[30] R. Polski, Y. Zhang, Y. Peng, H. S. Arora, Y. Choi, H. Kim, K. Watanabe, T. Taniguchi, G. Refael, F. von Oppen *et al.*, arXiv:2205.05225.

[31] M. Xie and A. MacDonald, Phys. Rev. Lett. **124**, 097601 (2020).

[32] E. Y. Andrei and A. H. MacDonald, Nat. Mater. **19**, 1265 (2020).

[33] T. Li, S. Jiang, L. Li, Y. Zhang, K. Kang, J. Zhu, K. Watanabe, T. Taniguchi, D. Chowdhury, L. Fu *et al.*, Nature (London) **597**, 350 (2021).

[34] A. Ghiotto, E.-M. Shih, G. S. S. G. Pereira, D. A. Rhodes, B. Kim, J. Zang, A. J. Millis, K. Watanabe, T. Taniguchi, J. C. Hone *et al.*, Nature (London) **597**, 345 (2021).

[35] H. Pan, F. Wu, and S. Das Sarma, Phys. Rev. B **102**, 201104(R) (2020).

[36] H. Pan and S. Das Sarma, Phys. Rev. Lett. **127**, 096802 (2021).

[37] N. Morales-Durán, A. H. MacDonald, and P. Potasz, Phys. Rev. B **103**, L241110 (2021).

[38] S. Ahn and S. Das Sarma, Phys. Rev. B **105**, 115114 (2022).

[39] A. Kerelsky, C. Rubio-Verdú, L. Xian, D. M. Kennes, D. Halbertal, N. Finney, L. Song, S. Turkel, L. Wang, K. Watanabe *et al.*, Proc. Natl. Acad. Sci. USA **118**, e2017366118 (2021).

[40] E. Khalaf, A. J. Kruchkov, G. Tarnopolsky, and A. Vishwanath, Phys. Rev. B **100**, 085109 (2019).

[41] H. S. Arora, R. Polski, Y. Zhang, A. Thomson, Y. Choi, H. Kim, Z. Lin, I. Z. Wilson, X. Xu, J.-H. Chu *et al.*, Nature (London) **583**, 379 (2020).

[42] A. Jaoui, I. Das, G. D. Battista, J. Díez-Mérida, X. Lu, K. Watanabe, T. Taniguchi, H. Ishizuka, L. Levitov, and D. K. Efetov, Nat. Phys. **18**, 633 (2022).

[43] F. Wu, E. Hwang, and S. Das Sarma, Phys. Rev. B **99**, 165112 (2019).

[44] X. Li, F. Wu, and S. Das Sarma, Phys. Rev. B **101**, 245436 (2020).

[45] S. M. Davis, F. Wu, and S. Das Sarma, Phys. Rev. B **107**, 235155 (2023).

[46] E. H. Hwang and S. Das Sarma, Phys. Rev. B **77**, 115449 (2008).

[47] S. M. Davis, Y.-Z. Chou, F. Wu, and S. Das Sarma, Phys. Rev. B **107**, 045426 (2023).

[48] E. H. Hwang and S. Das Sarma, Phys. Rev. B **99**, 085105 (2019).

[49] J. M. Ziman, *Electrons and Phonons* (Oxford University Press, Oxford, 1960).

[50] N. W. Ashcroft and N. D. Mermin, *Solid State Physics* (Cengage, Boston, 1976).

[51] H. Min, E. H. Hwang, and S. Das Sarma, Phys. Rev. B **83**, 161404(R) (2011).

[52] P. Coleman, *Introduction to Many-Body Physics* (Cambridge University Press, Cambridge, 2015).

[53] D. K. Efetov and P. Kim, Phys. Rev. Lett. **105**, 256805 (2010).

[54] L. Rademaker, D. A. Abanin, and P. Mellado, Phys. Rev. B **100**, 205114 (2019).